A numerical study of the impact of gravity and Marangoni force on the droplet distribution of hypermonotectic Al-Bi alloys

M. Gruber-Pretzler,[1] L. Könözsy,[1] F. Mayer,[1] M. Wu,[1] A. Ludwig,[1] R.H. Mathiesen,[2] P. Schaffer[3] and L. Arnberg[3]

[1]Dept. Metallurgy, University of Leoben, A-8070 Leoben, Austria
[2]SINTEF Materials and Chemistry, NO-7491 Trondheim, Norway
[3]Dept. Mater. Sci. Eng., Norwegian Univ. Science and Technology, NO-7491 Trondheim, Norway

Abstract

Both real time experimental observation and numerical modelling have shown similar patterns of melt convection and droplet motion of the secondary liquid phase ahead of the monotectic reaction front, during directional solidification of hypermonotectic alloys. Two major mechanisms are responsible for this: one is the buoyancy force induced sedimentation of droplets which is parallel to the gravity direction and the other is the Marangoni force induced droplet motion which is parallel to the temperature gradient direction. This paper tries to compare both experimental and modelling results, and to achieve improved understanding of the spatial phase separation phenomenon during hypermonotectic solidification processes. The real time observations were done by means of synchrotron X-ray video microscopy. The experiments were carried out on Al-6 wt%Bi alloys which were solidified directionally in a temperature gradient against the gravity direction. A similar unidirectional solidification process was simulated with a two-phase Eulerian model. In this model, the Bi-enriched droplets are considered as a secondary phase, different from the parent melt. Droplet formation by nucleation and growth, and the motion of droplets by the two above-mentioned mechanisms are explicitly considered.

Keywords: Hypermonotectic, decomposition, directional solidification, modeling, droplet motion, convection, phase distribution.

1. Introduction

The components of hypermonotectic alloys are completely miscible above the binodal temperature. As the temperature drops into the miscibility gap, the melt decomposes and droplets of a secondary liquid form. This decomposition process includes nucleation and droplet growth. As the temperature further drops below the monotectic point T_m, the monotectic reaction occurs, and the droplets are entrapped into the monotectic matrix. For industrial applications, a homogenous distribution of a soft minority phase in a hard matrix is desired. However, a macroscopic spatial migration of the minority phase seems unavoidable no matter whether the alloy solidifies under normal terrestrial conditions [1–3] or under reduced gravity [4–6]. The spatial migration of droplets can nowadays be observed *in situ* by a synchrotron X-ray video microscopy [7]. Two mechanisms are responsible for the droplet motion: gravity-induced sedimentation and Marangoni movement. A two phase volume-averaging model, based on the earlier work of Beckermann *et al.* [8–10] and Ludwig *et al.* [11–14] on equiaxed solidification, was developed to model both mechanisms [15,16]. Simulation offers the possibility and flexibility to analyze droplet migration caused by different mechanisms in detail. This helps understanding of the experimental findings. Although the experimental setup is a 3D problem, the simulation is done in 2D for a first qualitative comparison. At the moment it seems to be a good approximation for the study of the different flow phenomena but, in future, further work has to be done in order to study the influence of the more complex 3D situation of the experiments.

2. Experimental observations

The experiments were carried out on beam line ID22 at the European Synchrotron Radiation Facility (ESRF). Details about the experimental procedure were described elsewhere [7,18]. A binary (Al-6 wt.%Bi) alloy sample with thickness 0.2 mm, sealed between two glass sheets, was solidified in a vertical Bridgman furnace, where a constant temperature gradient (14.6 K/mm) against the gravity direction was applied. The sample was moved in the gravity direction with a constant pulling velocity (7.2 μm/s). Therefore, the sample solidifies unidirectionally from bottom towards top, as observed with the synchrotron X-ray microscopy (Figure 1). Ahead of the monotectic reaction front, the tiny Bi-droplets (dark round phase) move (or are brought by the convection flow of the melt) rapidly upwards. Due to

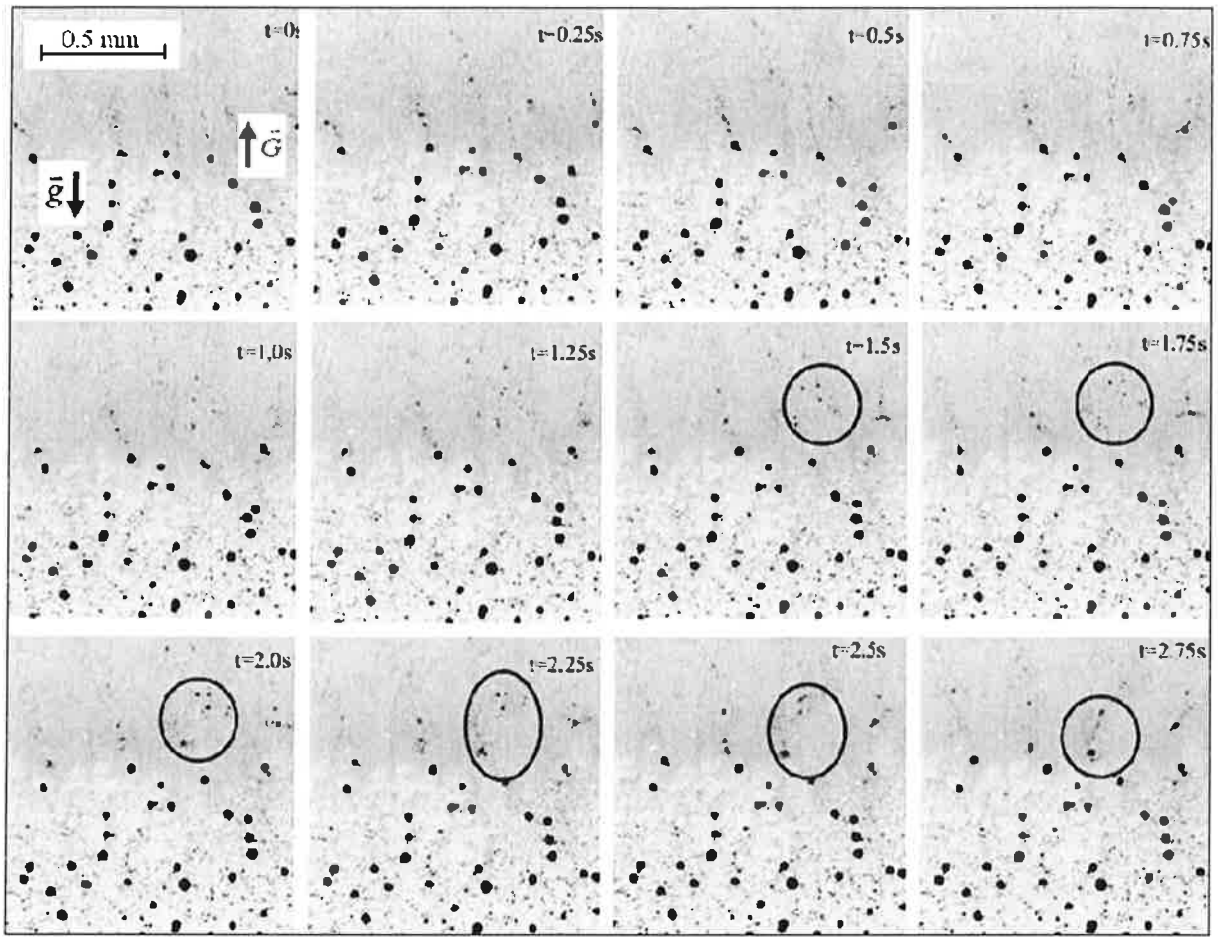

Figure 1: Unidirectional solidification of an Al-6 wt.%Bi alloy against the gravity direction. Vortices of the convective flow of the melt together with tiny Bi-droplets (seen as grey clouds) are observed just ahead of the monotectic reaction front. As the droplets grow to a certain size, they sink downwards due to gravity, and are finally engulfed in the monotectic matrix. Coagulation of the droplets, as highlighted in the circles, is observed from t = 1.5 s to 2.75 s.

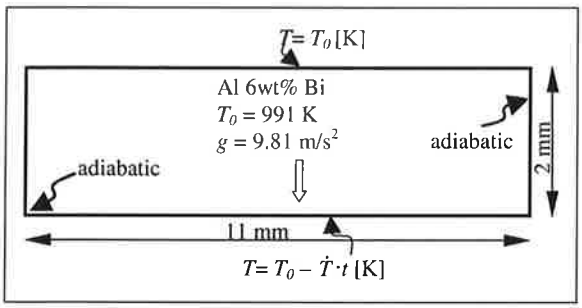

Figure 2: Scheme of the simulated case.

the drag force between melt and droplets, relative motion between the tiny droplets and the melt is too small to distinguish with the naked eye. The collective rise of the tiny Bi-droplets in the melt is inherently instable. It causes many local vortices just ahead of the monotectic reaction front, as in the Rayleigh-Taylor problem. When the droplets reach a critical size, they settle to the monotectic reaction interface, and are subsequently engulfed in the monotectic matrix. In addition to the diffusion-controlled growth of the droplets, the mechanism of droplet growth by coagulation is also evidenced as highlighted in the circles of Figure 1. The sedimentation of big droplets is caused by the large density difference between the Bi-droplets and the surrounding melt. The rise of the tiny Bi-droplets may be caused either by Marangoni force which is parallel to the temperature gradient [15–17], or by thermo-solutal convection of the melt. It is not possible to distinguish between those two mechanisms experimentally, so numerical studies are carried out as described in the following section.

3. Numerical simulation

In the applied numerical approach, four phases are considered to model hypermonotectic solidification: the parent melt (L_1) and the depositing secondary liquid phase (L_2) above the monotectic temperature T_m and below, the corresponding solidified monotectic matrix and the solidified secondary phase. A 3-parameter Gaussian distribution formulation is used to describe the heterogeneous nucleation of the L_2-phase as droplets. The growth kinetics (or droplet dissolution) is thought to be driven by diffusion. During monotectic reaction, the monotectic matrix is formed directly from L_1 enlarging the viscosity and releasing the latent heat of the monotectic reaction. The L_2 droplets approaching the monotectic reaction front are modeled to be entrapped in the monotectic matrix by applying a similar enlarged viscosity at/below the monotectic point. In

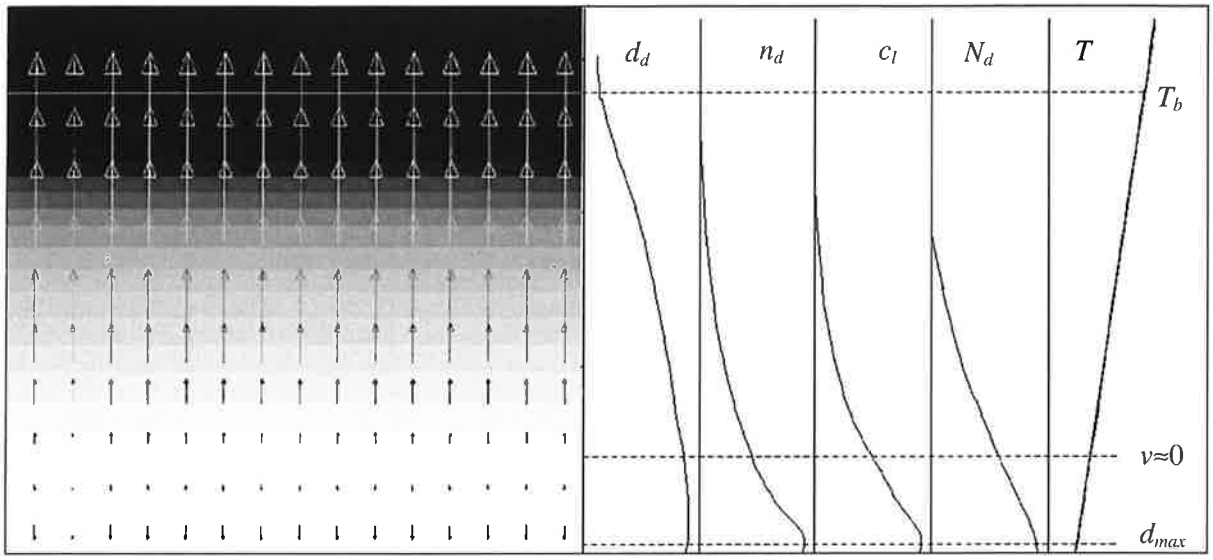

Figure 3: Left: a section of the calculation domain at t = 12.5 s after cooling starts. The contour plot of the droplet diameter is overlaid by the vector field of the droplets. The minimum droplet diameter d_{min} = 5.7 µm is shown in black whereas the maximum d_{max} = 11.5 µm is displayed in white. The velocity of the droplets varies between $v_{min} = 4 \cdot 10^{-6}$ m/s (black arrows) and $v_{max} = 1.4 \cdot 10^{-4}$ m/s (white arrows). The white line in the upper part of the picture shows the position of T_b. Right: distribution profiles along the casting direction of droplet diameter d_d, number density of the droplets n_d, melt concentration c_l, nucleation rate N_d and the temperature T. Small droplets move upwards, whereas bigger droplets move downwards.

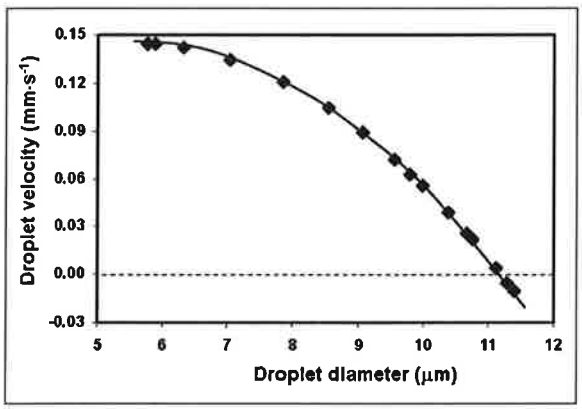

Figure 4: Correlation between the calculated droplet diameter and the droplet velocity.

addition, the following assumptions were made: (1) gravity induced sedimentation is modeled with a Boussinesq approach; (2) both liquid phases have the same viscosity; (3) the eutectic reaction of L_2 is ignored; (4) diffusion in a single droplet is infinite, and between droplets it is ignored; (5) no coagulation of droplets is considered currently. The mathematical equations used for this hypermonotectic solidification approach are summarized in [17]. The derivations of the numerical model and the numerical implementation of the model are described in previous publications [15,16].

With the information of the experiment in mind, a reduced 2D casting geometry is designed (Figure 2). The calculation domain of 11 x 2 mm^2 is meshed into volume elements of 0.1 x 0.1 mm^2. The boundary conditions are shown in Figure 2 as well. We start the cooling from an uniform initial temperature T_0 = 991 K. The bottom is continuously cooled with a cooling rate of $\dot{T}$ = 1.314 K/s. The temperature of the top is kept constant at T_H = 991 K till the monotectic temperature T_m = 930 K is reached at the bottom. The boundary conditions used are applied to mimic the unidirectional solidification experiments. The nucleation parameters for droplets are defined by a Gaussian distribution with a maximal nucleation rate $n_{max} = 5 \cdot 10^{12}$ m^{-3}, at an undercooling ΔT_N = 20 K, at which the maximal nucleation rate occurs, and a width ΔT_σ of the Gaussian curve = 8 K. For detailed information about the thermal physical properties and modeling parameters, the reader is referred to [17].

4. Results and Discussion

Nucleation of Bi-droplets starts as soon as the temperature drops below the binodal temperature T_b. The applied cooling conditions and the considered nucleation law lead to a maximum nucleation rate when the undercooling ΔT_N = 20 K below T_b is reached. Figure 3 shows one part of the calculation domain at t = 12.5 s. On the left hand side, the contours of the droplet diameter as the background are overlaid by the velocity vector field of the droplets. The minimum droplet diameter $d_{min} = d_{initial}$ = 5.7 µm is shown in black whereas the maximum diameter d_{max} = 11.5 µm is displayed in white. The velocity of the droplets varies between $v_{min} = 4 \cdot 10^{-6}$ m/s (black arrows) and v_{max} = $1.4 \cdot 10^{-4}$ m/s (white arrows). The position of the binodal temperature T_b is indicated by the white horizontal line in the upper part of the picture. On the right hand side, vertical cross sections of the droplet diameter d_d, number density of the droplets n_d, Al concentration of the parent melt c_l, number density of the nucleated droplets at this time step N_d (nucleation rate) and the temperature T are shown. Figure 4 shows the correlation between calculated droplet diameter and velocity of the droplets taken from the results of Figure 3. It is obvious that the maximum velocity occurs for the smallest droplets.

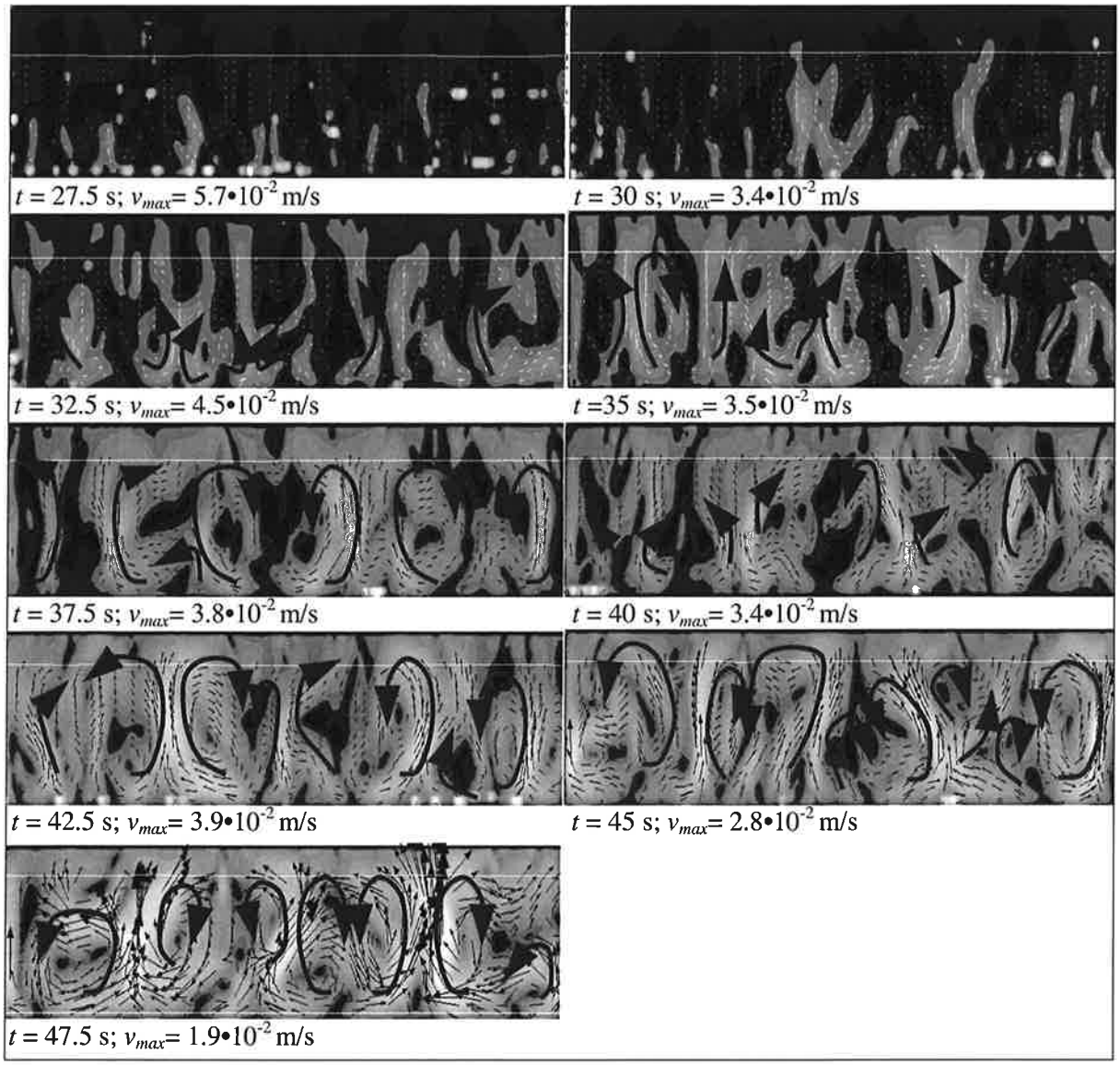

Figure 5: Velocity magnitude overlaid with the vector field of droplets: $v_{min} = 4 \cdot 10^{-6}$ m/s (short arrows, white areas) to $v_{max} = 2 \cdot 10^{-2}$ m/s (long arrows, black areas) at different calculation times. White line: isotherm of T_b; white line at the bottom: isotherm of T_m of $t = 47.5$ s.

Nucleation starts at the bottom of the sample. As soon as the small Bi-droplets nucleate, they start to move upwards due to Marangoni motion (upwards motion corresponds to positive velocity values, see Figure 3 and Figure 4). After the droplets are nucleated, they start to grow immediately. As they move upwards, they gain in diameter and therefore the influence of the gravity force on the droplet increases and leads to a decrease of the upward velocity. At a critical diameter, in our case this diameter is $d_{crit} = 11.2$ µm (Figure 4), the influence of gravity is so high that it overwhelms the Marangoni force. This then results in a change in direction of the velocity vectors. In fact, with further growth, gravity causes the droplets to move slightly downwards due to the density difference between the Al-rich melt and the almost Al-free droplets (Figure 3). While the Bi-droplets still grow, they sink and further nucleation leads to a continuous creation of new droplets besides the already existing ones depending on the calculated quantities, such as liquid concentration and temperature.

Figure 5 shows a sequence of the velocity fields for nine time steps, namely $t = 27.5$ s, 30 s, 32.5 s, 35 s, 37.5 s, 40 s, 42.5 s, 45 s, 47.5 s. The pictures show the magnitude of the velocity field of the droplets from $v_{min} = 4 \cdot 10^{-6}$ m/s (white areas) to $v_{max} = 2 \cdot 10^{-2}$ m/s (black areas) which is overlaid by the velocity vector field of the droplets by white (first four pictures) or black (last five pictures) arrows. Here the length of the arrows corresponds to the velocity magnitude. Again, the white almost horizontal lines in the pictures show the position of the isotherm T_b. Following the displayed pictures, the slow movement of the isotherm T_b can be observed and, at $t = 47.5$ s, the isotherm of the monotectic temperature T_m is appearing at the bottom of the picture. With that the solidification front is reached. As already mentioned, the relative motion in the melt is caused by its inherent instability which is referred to the classical Rayleigh-Taylor problem. The first two pictures in Figure 5 show slightly developing vortexes. Here the velocity of the droplets is still relatively small. With increasing cooling time, the velocity field starts to create more and more pronounced circulation. Black big arrows are used to visualize most of the vortexes.

Since the droplets grow further and further, the influence of the two included forces, gravity and Marangoni, increases the circulation in the calculation domain. After the third picture it is possible to follow the droplet movement to distinguish different vortices which develop in strength and geometry. Especially, in the last picture, the vortices start to get almost symmetric in shape and one could say that seven to eight circles have developed. Since the calculation domain has a length of 11 mm, in this specific case, the average diameter of one circle is about 1.3 mm.

5. Conclusions

A comparison of *in situ* x-ray video microscopy of a unidirectional hypermonotectic solidification process against gravity with a corresponding 2D numerical Eulerian-Eulerian approach was performed. In both experiment and simulation, periodic vortices form ahead of the monotectic reaction front. The simulation considers gravity and Marangoni force. Thermosolutal buoyancy was intentionally 'switched off'. Obviously, thermosolutal convection is not necessary to explain the complex flow pattern ahead of the monotectic front. Marangoni force drives clouds of tiny Bi-droplets upwards, while gravity moves bigger ones downwards. The collective rise of the small droplets together with the downwards motion of the big ones is inherently instable and hence induces the vortices. The average size of the vortices differs. We found 0.4 mm in the experiments and 1.3 mm in the simulations. This difference may be caused by thermosolutal buoyancy, droplet coagulation, transient or size effects (2D vs. 3D). Here, further numerical efforts are necessary.

Acknowledgment

This work was/is supported by the ESA-MONOPHAS project: "Advanced Bearing Alloys from Immiscibles with Aluminum".

References

1. L. Ratke and S. Diefenbach, *Mater. Sci. Eng. Rev.*, 1995, **R15**, 263.
2. B. Prinz, A. Romero and L. Ratke, *J. Mater. Sci.*, 1995, **30**, 4715.
3. J. Alkemper and L. Ratke, *Z. Metallkd.*, 1994, **85**, 365.
4. L. Ratke, G. Korekt and S. Drees, *Adv. Space Res.*, 1998, **22**, 1227.
5. L. Ratke and G. Korekt, *Z. Metallkd.*, 2000, **91**, 919.
6. H.U. Walter, *Proc. RIT/ESA/SSC Workshop: ESA SP 219*, 1984, p. 47.
7. P.L. Schaffer, R.H. Mathiesen and L. Arnberg, *Proc. MCWASP XI*, 2006, pp. 383–389.
8. C. Beckermann and R. Viskanta, *Appl. Mech. Rev.*, 1993, **46**, 1.
9. J. Ni and C. Beckermann, *Metall. Trans. B*, 1991, **22B**, 349.
10. A.V. Reddy and C. Beckermann, *Metall. Mater. Trans. B*, 1997, **28B**, 479.
11. A. Ludwig and M. Wu, *Metall. Mater. Trans. A*, 2002, **33A**, 3673.
12. M. Wu, A. Ludwig, A. Bührig-Polaczek and P.R. Sahm, *Internat. J. Heat Mass Trans.*, 2002, **46**, 2819.
13. M. Wu and A. Ludwig, *Adv. Eng. Mater.*, 2003, **5**, 62.
14. M. Wu, A. Ludwig and J. Luo, *Mater. Sci. Forum*, 2005, **475–479**, 2725.
15. M. Wu, A. Ludwig and L. Ratke, *Modell. Simu. Mater. Sci. Eng.*, 2003, **11**, 755.
16. M. Wu, A. Ludwig and L. Ratke, *Metall. Mater. Trans. A*, 2003, **34A**, 3009.
17. A. Ludwig, M. Wu, M. Abondano, L. Ratke, *Mater. Sci. Forum*, 2006, **508–509**, 193–198.
18. R.H. Mathiesen *et al.*, *Metall. Mater. Trans. B*, 2002, **33B**, 613. ■